Master RADMEP

Master *Radiation and its Effects on MicroElectronics and Photonics Technologies* (RADMEP)

COMPARISON OF HEAVY ION AND PULSED LASER SINGLE-EVENT EFFECT TEST DATA FOR ANALOGUE AND DIGITAL DEVICES

Master Thesis Report

Presented by

Annika Häkkinen

and defended at

University Jean Monnet

9.-10.9.2024

Academic Supervisor(s): Dr. Kimmo Niskanen

Host Supervisor(s): Dr. Richard Sharp, Dr. Chris Chong

Jury Committee:

Dr. Arto Javanainen	University of Jyväskylä
Prof. Dr. Guy Meynants	KU Leuven
Assoc. Prof. Dr. Adriana Morana	University of Saint-Etienne
Asst. Prof. Dr. Matteo Ferrari	University of Saint-Etienne

Erasmus+ UNIVERSITÉ JEAN MONNET SAINT-ÉTIENNE JYVÄSKYLÄN YLIOPISTO UNIVERSITY OF JYVÄSKYLÄ KU LEUVEN UNIVERSITÉ DE MONTPELLIER

Comparison of Heavy Ion and Pulsed Laser Single-Event Effect Test Data for Analogue and Digital Devices

Master's Thesis, 22.8.2024

Author:

Annika Häkkinen

Supervisor:

Kimmo Niskanen – University of Jyväskylä
Richard Sharp– Radtest Ltd
Chris Chong– Radtest Ltd

UNIVERSITY OF JYVÄSKYLÄ
DEPARTMENT OF PHYSICS

Abstract

Häkkinen, Annika
Comparison of Heavy Ion and Pulsed Laser Single-Event Effect Test Data for Analogue and Digital Devices
Master's thesis
2024

This thesis examines the comparison of heavy ion and pulse laser SEE testing in analogue (LM124 operational amplifier) and digital parts (23LCV512 SRAM). The testing was conducted for Radtest Ltd and the goal was to collect data for their pulsed laser testing system, SEREEL2. The heavy ion testing was done in Heavy Ion Facility at UCLouvain, Belgium. For the LM124, SET cross sections were calculated and presented as a function of LET. These results showed that the saturation started from around the LET of 30 MeV/(mg/cm^2) which was similar result to the literature. The pulse shapes from the laser testing were connected to specific transistors with the layout of the device and could be compared between heavy ion data. This comparison showed that the pulse shapes from the heavy ions were possible to be connected to specific transistors. The SET cross sections were calculated also for the most common pulse shape groups and they were presented with the different values of LET. For the 23LCV512, SEU cross sections – for both heavy ion and laser testing – were calculated and presented as a function of LET and laser pulse energy. Unlike with LM124, for the 23LCV512 the same test method did not transfer as well between heavy ion and laser testing. Thus the resulting SEUs were not triggered from the same area resulting in different formats of SEUs. As a solution for this, options like backside testing were discussed.

Keywords: Master's thesis, SEE Testing, Heavy Ion Testing, Pulsed Laser Testing

Preface

First of all, I would like to express my gratitude to my supervisors. Thank you to Dr. Richard Sharp, the CEO of Radtest Ltd, for giving me this opportunity and helping me along the way. I would also like to thank Dr. Chris Chong and Dr. Kimmo Niskanen for helping and supporting me with my internship and thesis work.

I want to thank my colleagues at Radtest Ltd for their help along the internship. Special thank you to Aditi who did long days with me to help me to graduate and with whom UK's rainy summer did not feel boring at all.

This program has helped me to find a field that I am interested in and all credit for that goes to my professors at all four universities. Thank you for the valuable and inspiring lectures you have given. Thank you also to the RADMEP organization for this unique opportunity and the financial support provided. I am also thankful for the UK Space Agency for funding my internship as a part of their SCIF project.

I would like to also thank my friends at RADMEP and all the friends from along the way who helped me create great memories and unforgettable times. Special acknowledgment has to be given to Alla for being an unwavering support and best possible friend in the most fun days as well as the worst ones.

Lastly, I would like to thank my friends and family who supported me through these last two years and never stopped cheering me on.

Annika Häkkinen

Contents

1 Introduction

Radiation testing is a crucial part of ensuring reliability and functionality of electronic components and systems even at the most radiation harsh environments. As radiation can cause damage and interference in the devices it is important to identify and minimize these possible issues. Space is one environment for which this type of testing is especially important as it is not easy to change the damaged parts in the middle of a space mission. If the parts are tested in advance it is possible to protect or change the radiation sensitive components and thus possibly save money and make the mission more secure. Space is not the only radiation harsh environment for which testing could be useful. Even in the atmosphere radiation can be an issue and for example high-altitude aviation can suffer from radiation effects.

The need for radiation testing keeps growing due to the development of the transistor design. The constantly reduced scaling of the transistors does have its advantages but it also has made the devices more and more sensitive to radiation effects. Testing for these effects has usually been done with particle accelerators. With these accelerators it has been possible to simulate effects normally only found in the more radiation harsh environments. Using the particle accelerators is a relatively reliable way of testing but it does have its limitations. Especially the limited availability and the high prices of the facilities has led to the need of developing alternative methods – one of these being pulsed laser testing.

Pulsed laser testing is an alternative radiation testing method. It is used especially as a complementary method besides accelerator based testing. The interest for developing pulsed laser testing comes from the fact that it is generally cheaper and more accessible. Also as a technical advantage the pulsed laser has normally smaller beam size so it is possible to focus the data acquisition better. However one of its most interesting advantages – especially when using the data as complementary to accelerator based data – is the possibility to collect spatial information and know the location of the effects.

Pulsed laser testing is an increasingly important method as the technologies used in the radiation harsh environments develop and with it the need for radiation

testing increases. Heavy ion testing is still very reliable and will not be easily – if ever – replaced but these alternative methods could work well as complementary methods. By doing radiation testing and damage evaluation partly with pulsed laser testing, it is possible to reduce the needed beam time. Pulsed laser testing can also provide better understanding of the functionality of the device before heavy ion testing. However, stronger understanding is still needed to be able to compare how the heavy ion and pulsed laser data correlate in different types of devices.

In this thesis both of the previously mentioned testing methods were used and the goal was to compare the data acquired from these measurements. In order to get different types of effects, the testing was done in both digital and analog device. The study was done for Radtest Ltd and thus the pulsed laser testing measurements were done with their testing system, SEREEL2. Important part of this study was to provide comparable data for the company for this particular system as well as continue the study previously started in the company. This internship was sponsored by UK Space Agency as a part of their SCIF project.

2 Theoretical Background

Radiation effects on microelectronics can generally be divided in three different groups – Total Ionising Dose (TID), Displacement Damage (DD) and Single–Event Effects (SEE) [1]. In this thesis the focus is on the SEEs. This section aims to provide an understanding of physical mechanisms behind SEEs and other key concepts used in this study.

2.1 Radiation – Matter Interactions

In this study focus was on heavy ion and laser testing so these interactions are looked more closely. Since these interactions have different influencing particles it is important to understand how this affects the interaction itself. Understanding the differences in particle level also helps to understand how heavy ion and laser testing can be compared.

Considering particle radiation, there are many possible ways for radiation to interact with matter. The type of interaction is dependent on the type and energy of the particles traveling through the matter. The energy loss that happens while the particle is traveling through the target material, can either happen via electronic or nuclear stopping. In electronic stopping the incident ion interacts with electrons from the target atoms and these electrons can be excited to a higher state. If the energy that the incident particle transfers to the electron is high enough, the electron can break away from the target atom thus causing ionization. With heavy ions, electronic stopping is the main reason for the ionization.[2, 3]

Radiation, such as photon, electron, proton and heavy ion radiation are all capable of ionization when interacting with matter. To understand these interactions it is important to explain the concept of Linear Energy Transfer (LET). LET describes the total ionization energy loss of incident particle per unit of path length in the target material. The usual unit for LET is presented as MeV/(mg/cm^2) and it reflects how densely the particle's energy is distributed along its path while it is traveling in the matter. The higher the LET value is the more the particle deposits energy per

distance to the material while going through it. [1]

Since laser consists mostly of photons for understanding of laser testing, photon-matter interaction is an important concept. Photons can interact with matter in several ways. First possibility is that the photons are deflected from the target atom electrons without the atom being effected. This is called Rayleigh's (or coherent) scattering. Other possibility is that the photon can produce an electron-positron pair. This can happen when the photon passes near enough of a particle with enough energy. Third possibility for the photon collision is Compton (or incoherent) scattering in which case a photon has more energy than the binding energy that holds an electron to its atom and thus it can knock the electron out of the atom. After this the photon may continue moving in a new direction with reduced energy. The final interaction between photons and matter is Photoelectric Effect (absorption). This is the effect that causes the ionization when photons are used – for example with laser. In photoelectric effect photon's energy is fully absorbed by an electron bound to an atom and the electron can be ejected from the atom. It occurs only if the photon's energy exceeds the binding energy of the electron in an atom. [2]

So when the heavy ions or photons interact with the matter they cause ionization via electronic stopping or photoelectric effect. The difference between the interactions causing the electron-hole pairs needs to be considered also when testing, because the testing will have very different contributors in each case. In heavy ion testing, ion energy and atomic number affect the ionization. With laser testing the charge generation depends on laser wavelength, focusing optics and photon density. [4]

2.2 Single–Event Effects

Single-Event Effects can occur in an electronic component as a result of highly energetic particle crossing the device through or near its radiation sensitive nodes. Ionization causes the particle's energy to be converted to charges (electron-hole pairs) across its path which can disturb the functionality of the device. In Fig. 1 the basic mechanism for the electron-hole pair production in semiconductor device is presented.

The effect caused by the particle might not be observable or it can occur for example as a change of the logic state in a memory device or as a transient disruption in circuit's operation. Depending on the device, the particle can produce different types of effects such as Single-Event Transients (SET), Single-Event Upsets (SEU),

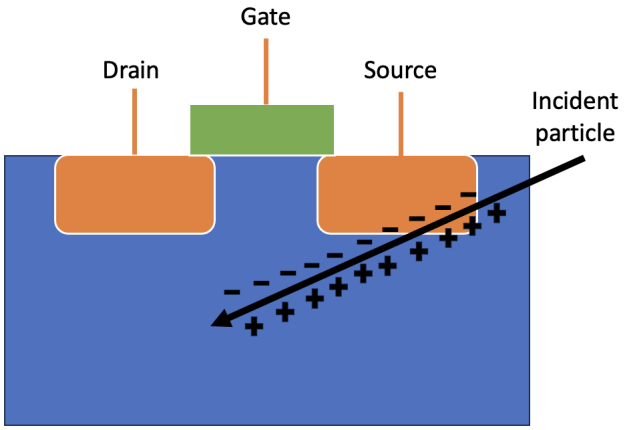

Figure 1. The formation of electron-hole pairs in a semiconductor device.

Single-Event Latchups (SEL) and Single-Event Burnouts (SEB). In this study we focused mostly on SETs and SEUs with a slight touch on SELs. [5]

Different types of SEEs can be divided into hard errors and soft errors. Hard errors are the kinds of SEEs that are non-recoverable. This means that the particle causes permanent changes in the integrated circuit. For example SEB and Single-Event Gate Rupture (SEGR) are considered hard errors. Soft errors on the other hand are the types of SEEs that can be recovered using different methods such as power cycling or rewriting the information. Soft error SEEs include the SETs, SEUs and SELs. [6]

In this thesis SETs are one of the main group of radiation effects studied. SETs are soft error SEEs that can momentarily change the nodal voltage or current in the integrated circuit [6]. These voltage or current transients can disrupt the functionality of the device. In Fig. 2 an example of SET induced voltage transients with different amplitudes are shown.

SETs affect the combinational gates of the circuit and it is also possible for SETs to propagate and be captured by a latch or a flip-flop in memory devices. If this kind of propagation happens, the state of a memory cell might change causing an error to occur when reading the memory. This kind of soft error is called Single-Event Upset (SEU). SEUs can be studied in memory devices – such as SRAMs – by writing a known content in the memory, and reading the memory during or after irradiating it. After this we can observe the amount of changes that happen compared to the written content and see the number of SEUs. [6]

SEU is a change in the memory device caused by a single particle. Depending

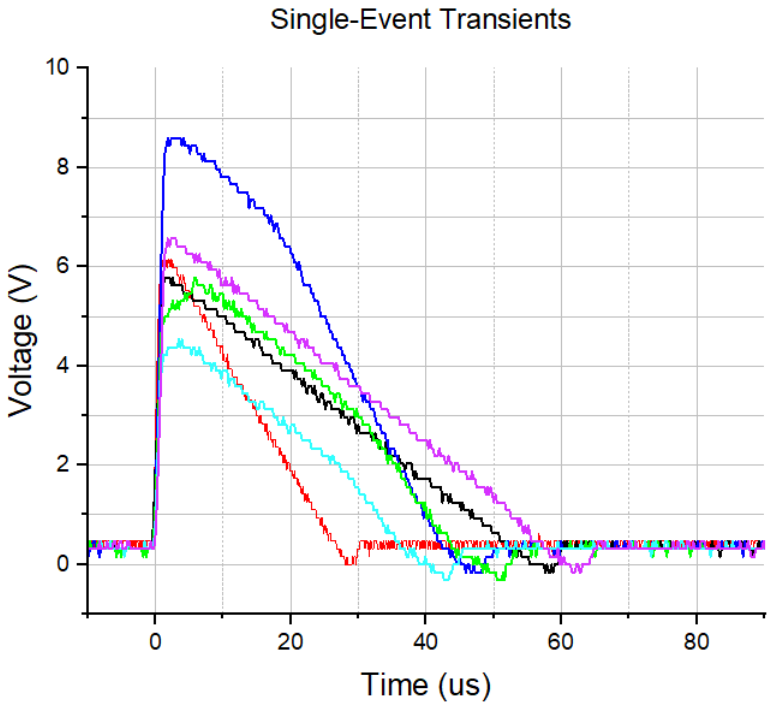

Figure 2. SET induced voltage transients with different amplitudes.

on the angle of the particle's path and the structure of the device we can have different kinds of changes in the memory. Sometimes one particle can cross several memory cells altering the content of all or some of these on its way. This is called Multiple-Cell Upset (MCU). Other possible way for the particle to cause an upset is for it to affect only one cell. In the case where only single SEU happens inside this cell and only one bit changes its state, we get a Single-Bit Upset (SBU). In some cases a particle can also change multiple bits inside the same cell. This is called Multiple-Bit Upset (MBU). [6]

In Single-Event Latchup (SEL) a low resistance path occurs between the power supply and ground. This causes high currents in the device which can be destructive if the current runs long enough. In these cases we can have for example melting in the silicon regions. However, SEL's destructive features can be avoided if the power is turned off immediately after SEL occurs. By power cycling we can return from the high current state back to the normal functionality of the circuit. [7]

2.3 Heavy Ion Testing

Heavy ion testing is a method used to evaluate the radiation sensitivity of electronic components and it can be used for SEE testing. In this kind of testing ions, such as xenon and krypton, are accelerated and directed at the electronic device. When these ions penetrate the material, they lose energy primarily through ionization. While passing through the device, the ions create tracks of electron-hole pairs as presented in Section 2.1. This ionization can induce transient currents, voltage transients, or even destructive events like SELs or SEBs. [8]

The purpose of heavy ion SEE testing is to obtain values for SEE cross-section at different LET values. As mentioned before, the ion type and its energy have to be chosen carefully in order to get specific LET value. Higher LET values correspond to more significant energy deposition and thus increase the likelihood of triggering SEEs. By changing the LET, it is possible to simulate different radiation environments and find possible thresholds for the SEEs. In addition to LET, other important parameters in heavy ion testing are flux (unit of ions/(s cm^2)) and the resulting fluence (unit of ions/cm^2). The relationship between these is important to relate properly. Flux is normally selected to be between 10^2 and 10^5 ions/(s cm^2) but it is important to make sure that the resulting fluence is not too high considering the sensitivity of the device. Also the time for the entire measurement should be designed to be reasonable by adjusting these two values correctly. [8]

As mentioned above, cross section is an important characteristics when studying the sensitivity of a device. Cross section can be defined with the number of events (N) and particle fluence (Φ) as follows

$$\sigma = \frac{N}{\Phi}. \tag{1}$$

Unit of cross section is defined as cm^2. Cross section can be defined for example for SETs or SEUs by using the obtained amount of these as the number of events. [8]

The error for cross section can be estimated with division error formula [9]. For cross section calculation the formula would be as follows

$$\delta\sigma = \sigma \cdot \sqrt{(\frac{\delta N}{N})^2 + (\frac{\delta \Phi}{\Phi})^2}. \tag{2}$$

In this equation $\delta\Phi$ is the estimated error for the fluence and δN is the estimated

error for the events. If the number of events can be assumed to follow Poisson's distribution – as presented in [10] – the equation for the error of the number of events is as follows

$$\delta N = 1.960 \cdot \sqrt{N}. \tag{3}$$

Heavy ion testing – as most experimental methods – does have its limitations. Sample preparation and possible decapsulation of the device might be needed in order to reach the sensitive areas. Also heavy ion testing is expensive and often requires traveling since the amount of facilities is limited. Beam time is also regulated and not always easily accessible. In the technical side another limitation for some experiments is the lack of spatial data, meaning that it is impossible to know in which area of the device the SEE happens. [4]

2.4 Pulsed Laser Testing

Even though heavy ion testing is the most common way to study SEEs, the limited beam time and high cost have increased the study of alternative methods. Pulsed laser testing is meant to be more in-lab-experiment which means it saves money, time and is more accessible. In addition to these advantages, with pulsed laser comes the possibility to obtain spatial information. This feature can be useful also when combining both heavy ion and pulsed laser data. [4]

In pulsed laser testing, laser system generates extremely short pulses of light and these light pulses are directed to the device. The pulses are normally in the scale of nanoseconds up to picoseconds but with today's technology it is possible to go down to femtoseconds [11]. Once the device is shot with the laser, photon energy is absorbed by the material which creates localized ionization and electron-hole pairs [12]. As stated previously the electron-hole pairs can lead to transient currents and voltage transients meaning that SETs can happen.

2.4.1 Absorption Mechanisms

Since laser consists of light, photons are responsible for the creation of electron-hole pairs and the mechanism for this is absorption. There are two types of absorption mechanisms depending on the energy of the photon. Single-Photon Absorption (SPA) – also known as linear absorption – happens when the energy of the photon is higher than the bandgap of the semiconductor (usually looking at silicon with the bandgap of 1.12eV). The basic principle of SPA is that an electron in the penetrated material absorbs the photon and is excited to a higher energy state. The process is called linear because of its linear relationship with light intensity, meaning the absorption is directly proportional to the number of photons present. In SPA the photons are absorbed one by one. [4]

The second possible process for the absorption is called Two-Photon Absortion (TPA) or non-linear absorption. TPA happens when photon energies are less than the bandgap value. As its name suggests, in TPA two photons are absorbed, each carrying half of the energy needed to match the bandgap, and their simultaneous absorption leads to the excitation of an electron. This process requires a significantly higher light intensity and is non-linear because the absorption rate depends on the square of the light intensity. When comparing these two absorption methods it is important to note that SPA is always dominating if there is a possibility for both SPA and TPA. Whether it is sensible to use SPA or TPA can depend on several factors. For some applications TPA is more suitable as it offers better spatial resolution and deeper penetration depth. However, since SPA always dominates when both of them are possible, TPA does require high optical intensity (for example femtosecond pulses). [4]

One important concept for the understanding of pulsed laser testing is front-side and backside testing. These are two techniques with which laser testing can be approached. Front-side testing is more simple out of these two. In this technique the laser beam is focused on the sample through the top layers, meaning that preparation for this type of testing only requires the removal of the packaging and possibly the cap or lid of the device. In front-side testing SPA is commonly used method because it allows direct interaction with the active layers, enabling precise measurements of the device's optical and electronic characteristics. [13]

Even though front-side testing is the more simple approach when it comes to the preparation of samples, it is not always possible to obtain results this way. In

today's technologies density and amount of metal layers has increased which means there are often areas that the laser can not penetrate from the front-side. In these cases backside testing is the preferred method. In backside testing the laser beam is focused to the backside of the device and the active layers are reached through the substrate. Both front-side and backside testing principles are presented in Fig. 3. This does require more sample preparation as the backside needs to be opened and the surface has to be polished to mirror quality in order to get uniformed beam quality. For the backside testing it is possible to use TPA or high wavelength SPA.[4, 13]

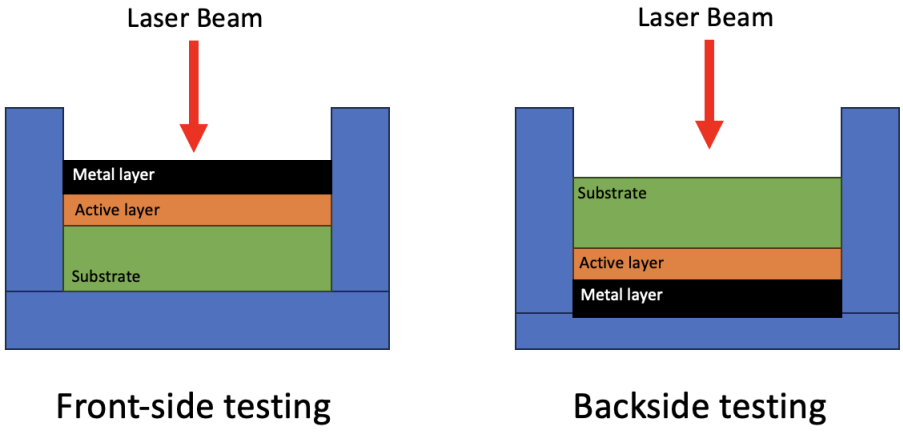

Figure 3. Presentation of the differences between front-side and backside testing.

2.4.2 Key Parameters of Pulsed Laser Testing

In laser testing there are several parameters that need to be considered in addition to the testing technique. Wavelength is one of the most important parameters which effects also the choice of SPA or TPA. For backside testing it is needed to use longer wavelengths in order to get deep enough penetration. For TPA this means at least the wavelength of 1260 nm and for SPA 1064 nm, respectively. If the front-side testing is chosen as a method, shorter wavelength can be possible for SPA. However, usually for silicon devices the standard wavelength is 1064 nm even in the front-side testing. This is due to its deep penetration length even when using SPA and the availability of Nd:YAG lasers which use this wavelength. As a parameter, wavelength is facility specific and often laser testing systems offer several options for this. [4, 14]

Another important parameter in laser testing is pulse width. This means the duration of one laser pulse and there are few conditions for this parameter. Since the goal of the laser testing is to produce as similar as possible SEEs compared to the heavy ions, it is important that the pulses are short enough. For one high energy ion it takes approximately 1 ps to travel through the junction in a circuit and this time is much shorter than the typical response time in circuits. Similarly the laser pulse must be shorter than the response time in order to obtain valid results. The usage of ps lasers has made the laser testing more reliable and as mentioned before, the current development has also increased the usage of femtosecond lasers. [12]

Third crucial parameter in laser testing is beam spot size. Even though the spot size will always be larger than the heavy ion track, the goal is to make the spot size as small as possible. Microcsope objective is used to focus the laser beam to the spot area. When the objective lens is decided, we can also obtain a value for numerical aperture (NA), which is the product of refractive index and sine of the angle of incidence. When the wavelength (λ) and the numerical aperture are set, it is possible to calculate the spot size for the measurement with the following equation

$$R = \frac{1.22\ \lambda}{NA} \tag{4}$$

in which R gives the diameter of the spot size. As seen from this function, the numerical aperture has a big effect on the spot size. In order to get as small of a spot as possible it is important that the used objective has large incident angle, making also the numerical aperture large. [15]

Besides these three parameters, there are two parameters that are often varied more during the laser testing. These are pulse energy and pulse frequency. Pulse energy is often the main variable in the pulsed laser measurements and it can be varied relatively easily. For the pulse frequency – or also known as pulse repetition rate – the affecting factors are the scanning speed and the characteristics of the device under test. For the pulse frequency it is important to know the response time of the device in order to tune the repetition rate so that the pulse period is long enough for the device to return to its regular state. [4]

2.4.3 SEU Cross Section Calculation

In pulsed laser testing, fluence is not obtained in the same way as in heavy ion testing. In the case where cross section is required, some estimation is needed for the fluence. In [16] for the cross section the following equation was given

$$\sigma = N \cdot \frac{S}{\#Pulses} \tag{5}$$

where N is the number of events, S is the scanned area and $\#Pulses$ represents the number of pulses. In the case where total number of pulses is unknown it can be determined with the frequency (f) and total scan time (t_{scan}) as follows

$$\#Pulses = ft_{scan}. \tag{6}$$

When combining these two equations we get the equation for the pulsed laser cross section

$$\sigma = N \cdot \frac{S}{ft_{scan}} \tag{7}$$

By comparing the equation 7 to the equation 1 we can see that the equivalent fluence in the pulsed laser testing compared to the heavy ion fluence measurement is

$$\Phi = \frac{ft_{scan}}{S}. \tag{8}$$

3 Experimental Methods

In this section the experimental methods and measurement setups are explained. For this thesis we did measurements for two different devices – LM124 quad operational amplifier and 23LCV512 SRAM memory. Both devices were studied by using both heavy ion and laser testing.

3.1 LM124

In this study the analogue device used was LM124 which is a device often used when comparing the heavy ion and pulsed laser data. LM124 consists of four operational amplifiers and it is a linear circuit. The focus was on one of the four amplifiers and the goal was to use the transistors inside the amplifier in order to categorize and identify the SETs obtained from the heavy ion and laser testing. In Fig. 4 the circuit diagram is shown for one of the four amplifiers [17]. In these measurements the used LM124 was manufactured by Texas Instruments.

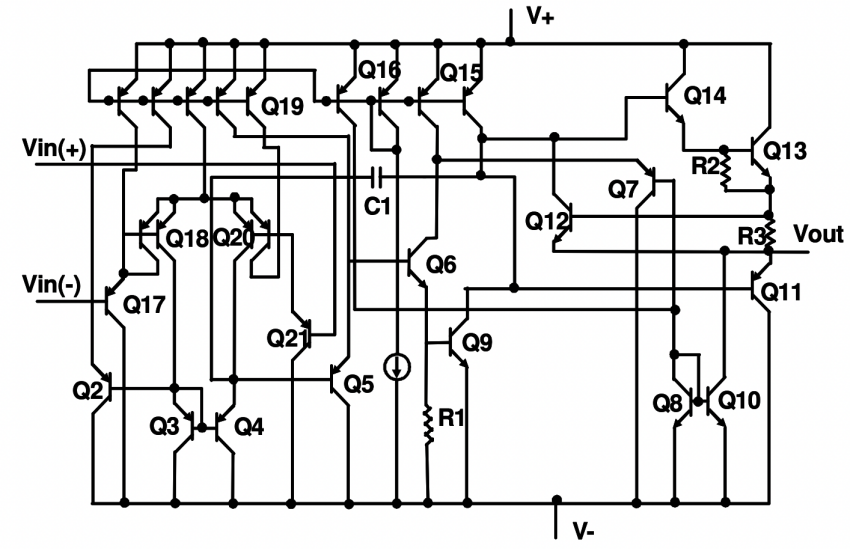

Figure 4. Circuit diagram of LM124 operational amplifier. © 2008 IEEE [17].

In order to power up the amplifier it was connected to a voltage follower circuit board, which is shown in Fig. 5. The output from this board could be collected from

the test pins connected to each operational amplifier. The output voltage received was half of the supply voltage and it was possible to give the board either single or dual supply.

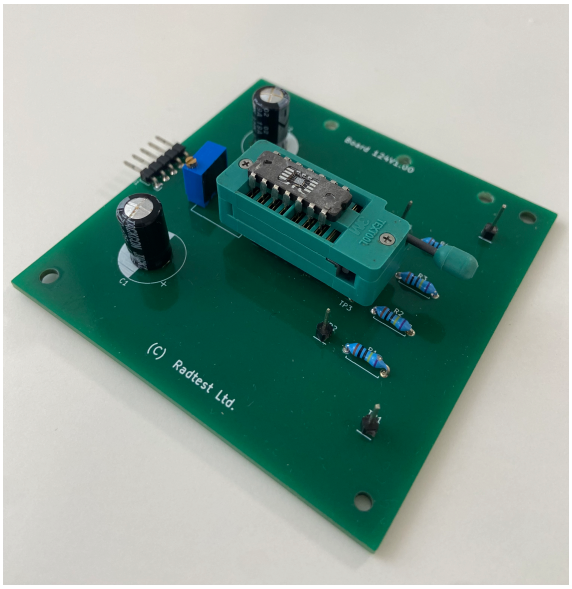

Figure 5. LM124 operational amplifier attached to the board used for the testing.

3.2 23LCV512 SRAM

As other part of this study focus was on a digital device called 23LCV512 SRAM. This device is a 512-Kbit serial memory with the organization of 64K x 8-bit. This SRAM uses the Serial Peripheral Interface (SPI) protocol to access the memory and since the 23LCV512 is designed to communicate directly with the SPI, it was possible to use direct SPI-to-USB connection to get the data from the memory. The device we used was manufactured by Microchip. [18]

The board used to obtain data from the device is shown in Fig. 6. A supply voltage was provided to the board and the communication with the memory, as well as with the output, was managed via SPI. The SPI required a clock input (SCK), data input (SI) and data output (SO), which were controlled by the fourth connected signal, chip select input (CS). The pins for all of these signals were included on the board. Additionally, a ground pin was added to the board, and the ground wire from the SPI connector was used.

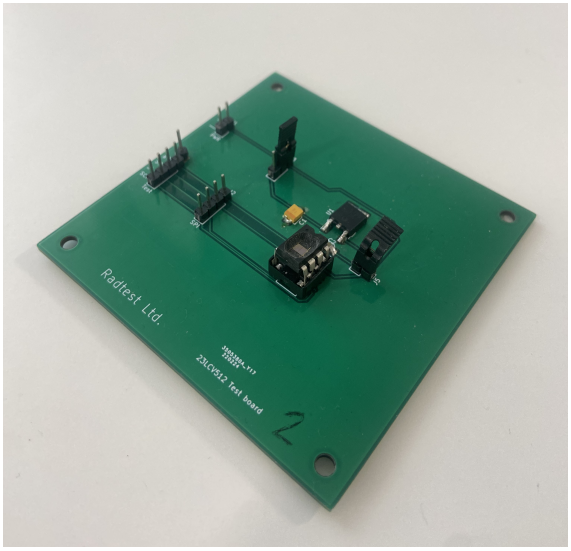

Figure 6. 23LCV512 SRAM attached to the board used for the testing.

The SRAM study was a continuation for a previous study done inside the company. The goal was to build more data on top of the previously acquired data and thus use the same device and test method. Previously for the SRAM the study was done only with heavy ions so the test method was designed just for heavy ion testing in mind. The previous data as well as the codes used for the SRAM study were received from private communications with Radtest Ltd.

3.3 Heavy Ion Test Setup

In this study the heavy ion testing was done in UCLouvain, Belgium. UCL's Cyclotron Resource Centre (CRC) uses CYCLONE multiparticle cyclotron. CYCLONE has several beam lines from which we used the heavy ion facility (HIF). HIF offers ions from carbon (LET = 1.3 MeV/(mg/cm^2)) up to xenon (LET = 62.5 MeV/(mg/cm^2)) and these heavy ions are produced with an external Electron Cyclotron Resonance (ECR) source. The LET values for the ions used in this study are shown in Table 1. After acceleration, the different ion types are extracted either with adjusting the cyclotron magnetic field or by changing the RF frequency. The irradiations in HIF are done inside a vacuum and the flux is possible to adjust from few ions/(s cm^2) up to $1.5{\cdot}10^4$ ions/(s cm^2). Other important parameters in HIF are the irradiation area diameter (25 mm) and the ion change time (15 min). [19]

Ion	LET (MeV/(mg/cm^2))
Carbon	1.3
Neon	3.3
Aluminium	5.7
Argon	9.9
Krypton	32.4
Xenon	62.5

Table 1. The LET values of the ions used in this study.

3.3.1 Heavy Ion Test Setup for LM124

For the LM124 heavy ion testing, the boards were placed inside the vacuum, and the board connections were wired to the outside equipment. The used board and the connections placed inside the vacuum can be seen in Fig. 7. The board was connected to two different power supplies to achieve a dual supply. Measurements were conducted with two different dual supply voltages. First, the supply voltages were set to -5 V and +5 V, and for the second set, -10 V and +10 V were used. Out of these dual voltages the analyzing was later conducted for the ±10 V sets due to the bigger transients we acquired with these voltages. Two test pins (out of the four possible amplifiers) were connected to a PicoScope to obtain waveforms, which served as the output. The measurement setup is presented as a block diagram in Fig. 8.

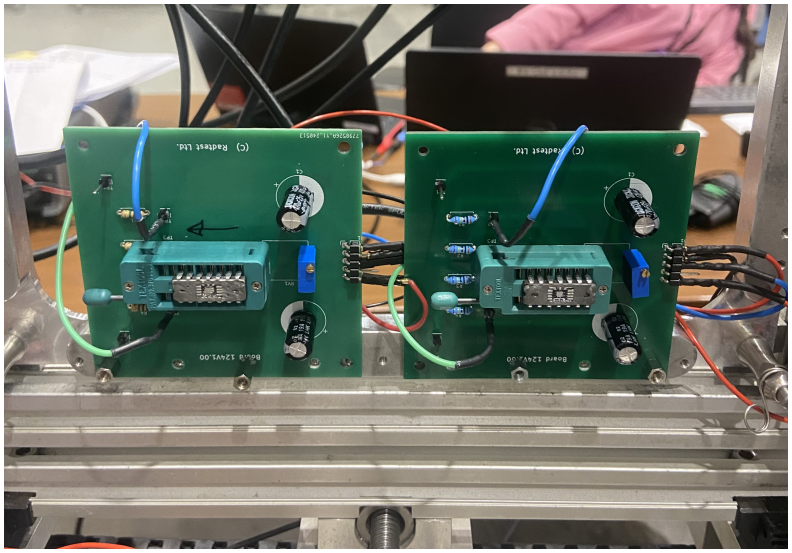

Figure 7. The board connections for LM124 inside the vacuum.

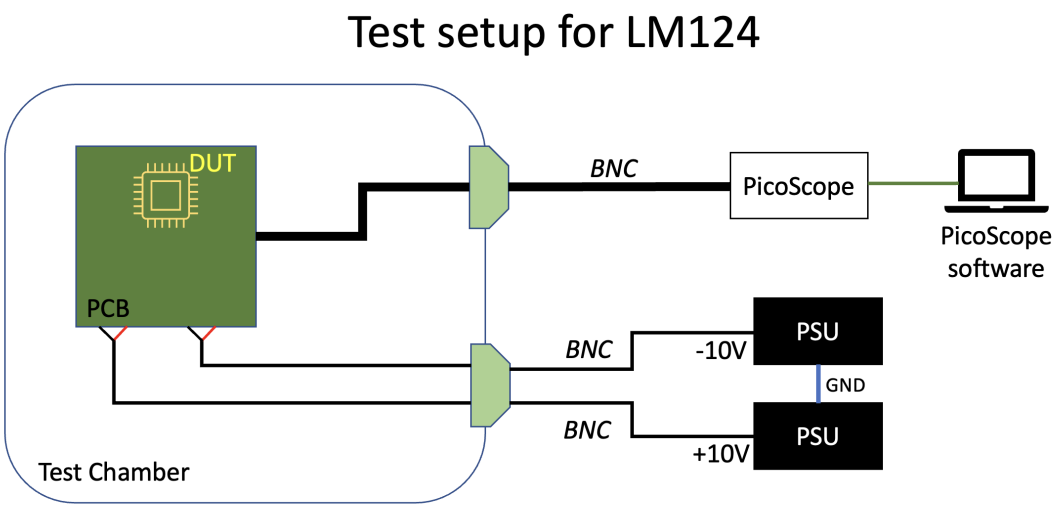

Figure 8. Block diagram presenting the setup of the LM124 testing.

Measurements were conducted by applying the supply voltage to the board and turning the beam on. The flux was set to the maximum ($1.5{\cdot}10^4$ ions/(s cm^2)), and the fluence was set to 10^6 ions/cm^2 for all LM124 measurements. The test was run until the target fluence was reached. The device was irradiated with five different ions: carbon, neon, argon, krypton, and xenon. The LET values of these ions can be seen in Table 1. Transients were obtained with all ions except neon. The obtained waveforms were saved and analyzed later with different methods.

3.3.2 Heavy Ion Test Setup for 23LCV512

For the testing of the digital device – 23LCV512 – the SPI was wired to the board inside the vacuum and the board was connected to power supply wires. The board connections for the 23LC512 inside the vacuum are presented in Fig. 9. The power supply was controlled with STS code, which is Radtest Ltd's system controlling software. With the STS code the board was given voltage of 3,3 V and current was limited to 5 mA. The STS code was used to guard the device from the cases where Single-Event Latchup might happen. In this situation the STS code turns the power supply off before the latchup can damage the device. Outside the vacuum the SPI was connected to C++ code which controlled the SPI and collected the SEUs. After collecting the SEUs, the number of SEUs could be calculated from the raw data by using SEU calculator made with Python. In Fig. 10 the setup is presented as a block diagram.

Figure 9. The board connections for 23LCV512 inside the vacuum.

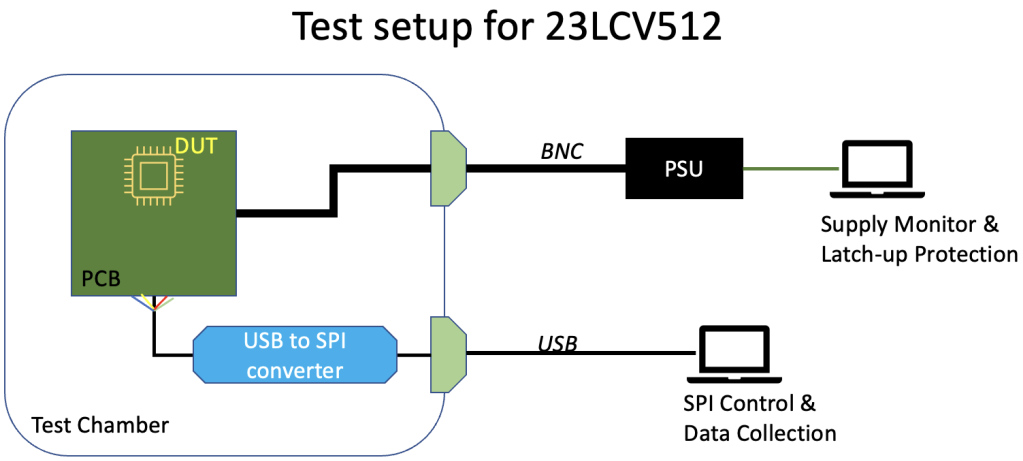

Figure 10. Block diagram presenting the setup of the 23LCV512 testing.

SEU data collection protocol was started by reading the memory once with the C++ code. After this the next step was to write a checkerboard pattern (01010101) in to the memory. As mentioned before the memory has 64K x 8-bit organization so the addresses had eight bits in total and the write function placed 01010101 pattern in them. This corresponds to decimal number of 170. When the beam was turned on during the measurement, the code was set in continuous read-write-mode. In this mode the code kept writing the checkerboard pattern to the memory and before each write command the memory was read and the addresses were saved. If SEU happened, the decimal value of the affected address would change from 170. This is how the SEUs were captured and with the Python code it was possible to calculate how many times the value 170 was changed by looking at the read files obtained from the measurement.

The SRAM was tested with three ions – carbon, neon and argon. The LETs for these ions can be seen in Table 1. From the company's previously acquired data it was possible to see the flux and fluence values that gave SEUs without triggering SELs. From this previous data it was possible to see that the 23LCV512 was much more sensitive than the LM124 and the flux and fluence could not be as high without latchup happening. This is why the study was started with the flux of 10^3 ions/(s cm^2) and the fluence of 10^5 ions/cm^2. These values worked well for the ions with the lower LETs (carbon and neon). However, for argon this value of flux triggered SEL immediately before any SEU data was obtained. This is why the flux was set to $8{\cdot}10^2$ ions/(s cm^2) and the fluence was set to $4{\cdot}10^3$ ions/cm^2. With this flux and fluence it was possible to avoid SEL and obtain SEUs for argon as well.

In the heavy ion experiments the previously stated test method was used for all three of the ions and the test was run until the target fluence was reached or a latchup happened. The read files were then read through the Python SEU calculator from where the amount of SEUs was observed. This data was analyzed with the Radtest Ltd's previously acquired data. This previous data included more SEU data for carbon and neon and in addition it had data for aluminium which was a useful addition since its LET is 5.7 MeV/(mg/cm^2) which is between neon and argon (Table 1). Because of the limited beam time it was not possible to acquire data from more than three ions, so the previous data was useful in order to get wider range for the analysis.

3.4 Pulsed Laser Testing

The laser testing part in this study was done with SEREEL2 pulsed laser testing system in Radtest Ltd's own facility. SEREEL2 is meant for simulating the impact of heavy ions and to make it possible to do radiation testing without particle accelerators. The high cost and limited availability of beam time are two important reasons for the need to improve laser testing possibilities. SEREEL2 has also the advantage of higher controllability compared to heavy ion testing as we are able to choose more precisely where the laser is targeted. SEREEL2 system is shown in the Fig. 11.

Figure 11. A) SEREEL2 pulsed laser testing system B) Closer image to the inside of the SEREEL2 system.

In SEREEL2 – as in laser testing often – it is possible to change certain parameters. For the objective lens the options are 5x, 20x, 50x and 100x and in this study for that the choice was 50x lens. Other parameters used for all the measurements in this study, were the wavelength of 1064 nm and the numerical aperture (NA) of 0.65. The pulse duration was set to the width of 200 fs. For the study of the digital device the pulse frequency was set to 200 Hz. The scans were done with Single-Photon Absorption.

The parameters that were varied between the measurements were the step size and pulse energy. For the step size the values of 2 μm and 5 μm were tested but all the final scans were done with the spacing of 2 μm. For the digital device the pulse energies were varied between different measurements to get comparison data from these values. The pulse energies were changed from 1 nJ up to 6 nJ.

With the known wavelength and numerical aperture the spot size of the laser can be calculated. For this, the equation 4 is used and the following value can be obtained

$$R = \frac{1.22 \cdot 1064nm}{0.65} = 1.9970...\mu m$$

$$R \approx 2.00 \cdot \mu m$$

This equation gives the lateral diameter of the spot size and this spot size was used in all the measurements. All the laser testing parameters are shown in Table 2.

Pulse duration	200 fs
Wavelength	1064 nm
Pulse frequency	200 Hz
Numerical aperture	0.65
Spot size (diameter)	2 μm
Step size	2 μm
Pulse energy	1–6 nJ

Table 2. The laser testing parameters used in this study.

For the operating system and user interface, SEREEL2 is combined with a software called SEESIM. SEESIM can be used for defining scan patterns, scan rates and pulse energies. It can also be used for analyzing the results and studying the heat map of the device.

3.4.1 Pulsed Laser Test Setup for LM124

Because LM124 is a quadruple operational amplifier it was possible to focus just on one of the four amplifiers since it can be assumed all four amplifiers would have the same response. By scanning only one amplifier, a lot of time was saved compared to scanning through the entire chip. In this scan the pulse energy was 2.06 nJ. Other parameters were the same as shown in Table 2. In Fig. 12 is presented the measurement setup for the LM124 testing inside the SEREEL2. The setup was built in the exact same way as for the heavy ion testing and the block diagram presentation of this is shown in Fig. 8. In this setup two different voltage sources were used in order to give the device the dual voltage of ±10V and the output test pins were connected to a PicoScope that collected the transients as voltage pulses.

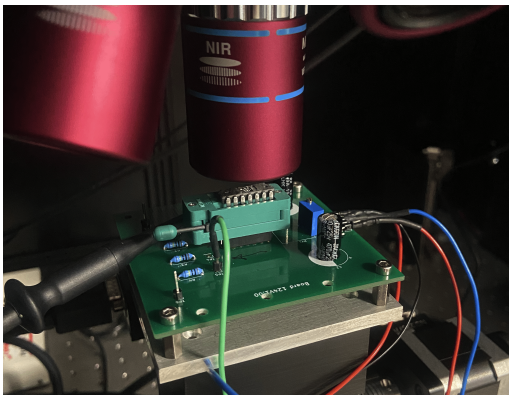

Figure 12. LM124 board setup inside SEREEL2.

In Fig. 13 is presented the heat map of the device. In this map the voltage transients are seen so that the darkest red color represents the amplitudes up to 10 V – whether going positive or negative – and the lightest blue is closest to zero, meaning that these areas have no voltage peaks. The map was created with SEESIM and with this system it was possible to analyze and see the transients by clicking the wanted area in the heat map. In this map it is possible to see already some possible positions for the sensitive transistors but this is compared more in Section 4.

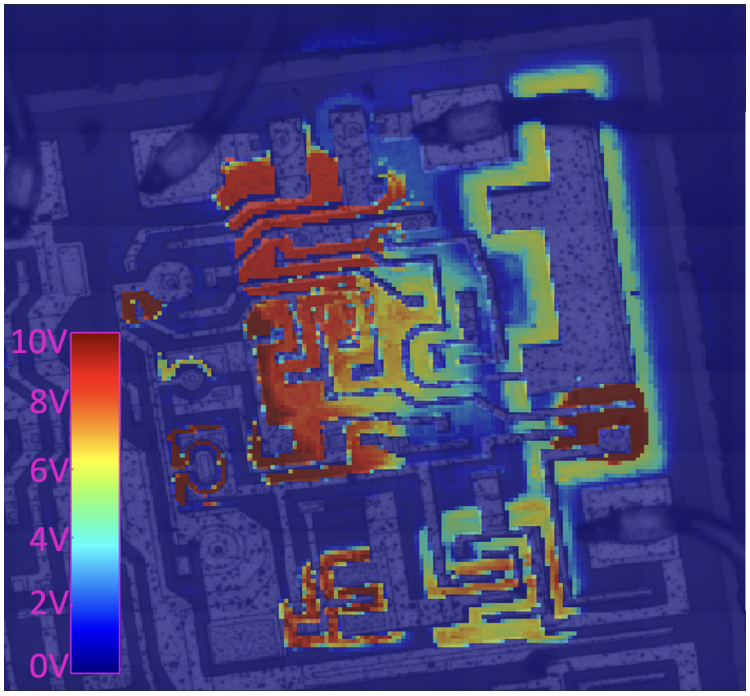

Figure 13. Heat map image of LM124 after the pulsed laser scanning with SEREEL2. The zero level of voltage is shown in blue and high voltage transients (up to 10V) are presented with the deep red color.

3.4.2 Pulsed Laser Test Setup for 23LCV512

For the testing of the 23LCV512 the same codes and basic methodology used in heavy ion testing were employed. The power supply was controlled again by using the STS code, which provided the board the voltage of 3.3 V and limited the current to 5 mA. The read-write methodology was implemented using C++ code, and SEUs were collected accordingly. The saved data files were processed through the Python code to calculate the number of SEUs. This measurement setup was presented in Fig. 10. Just like with the heavy ion data, the checkerboard pattern was used as a reference, and a change in the decimal number 170 indicated that SEU had occurred. In Fig. 14 the 23LCV512 board and the device are shown inside the SEREEL2 system.

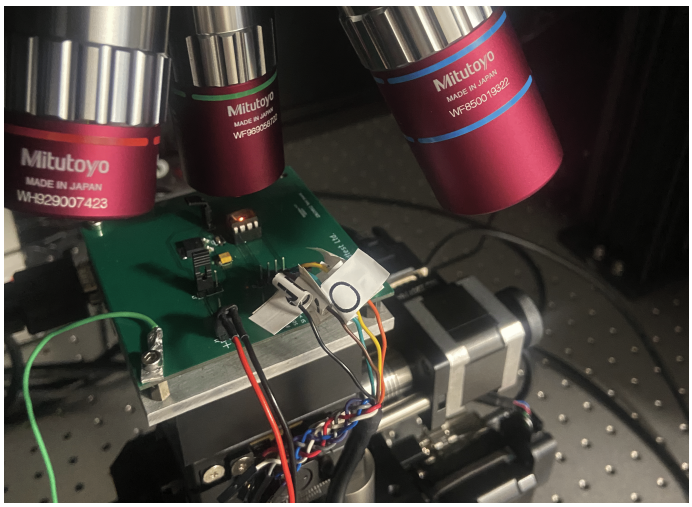

Figure 14. The 23LCV512 board setup inside SEREEL2.

For the laser testing of the 23LCV512 some things needed to be taken into account since the previous study – for on top of which this study was built – was only designed for heavy ion testing. Also it needed to be taken into account that the structure of the chip was fairly unknown so it was not clear where the sensitive areas were. With LM124 it was possible to focus on just one amplifier since the amplifiers have the same functionality between each other. This way it was possible to save scanning time. With 23LCV512 there was not as clear areas that could have been eliminated from the scan due to similarities. It also would not have been time efficient to scan the entire device multiple times with different pulse energies, so in the beginning of the study the sensitive areas had to be located.

The device was initially examined by conducting few scans in the areas with different textures to determine if SEUs could be found. After some SEUs were obtained with a pulse energy of 4.08 nJ, the entire board was scanned in ten sections to identify the exact sensitive area. It was discovered that SEUs were obtained only from the side of the chip which is shown as blue color in Fig. 15. The mosaic layout in this figure has been built with the mosaic assembling code further described in Section 3.4.3.

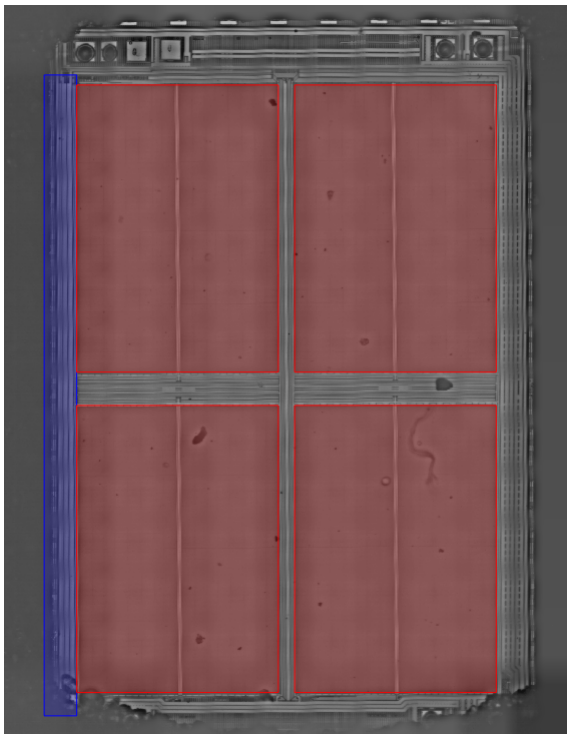

Figure 15. The layout of the 23LCV512 with the sensitive area marked in blue and the memory cell areas marked in red.

Once the area was narrowed down, it was scanned multiple times with four different pulse energies: 1.01 nJ, 2.13 nJ, 4.08 nJ, and 6.23 nJ. After collecting the data, it was put through the Python SEU calculator and it was noted that SEUs were found with all the pulse energies except for 1.01 nJ. Other than the pulse energy, the parameters remained the same as shown in Table 2.

Since the C++ code for SEU collecting was designed for heavy ion testing it was not perfectly synchronized with the laser scanning. The C++ code was slower at reading and writing the data than the laser was at scanning the chip. The dead time caused by the code was approximately half of the read time (2 s) and half of the

write time (0.6 s). This is because SEU can happen while the read or write time is going on and the SEU could be in these cases either not read or written on top of. Some dead time also came from the time it took for the code to change between the read and write operations. One possibility for tuning the code and the laser to match, would be to make the laser scan slower, but due to time limitations this was not possible. Also in this study the main point was to see the overall behavior of the SEUs in the digital device and the dependence of the different pulse energies.

3.4.3 Mosaic Image of LM124

As a part of this master's thesis one goal was to build a software application for the mosaic tiling of the images acquired from the laser scanning. In the laser scanning the chip area is filmed in tile images. Since the laser scanning step size often does not align perfectly with the image sizes, the tiles can not be built together by simply placing them next to each other. In the case that the step size is smaller than the images, the image tiles need to be overlapped with each other to create the perfect mosaic image. Matlab code created during this internship was able to take a folder with the tiled images and create a mosaic as long as the overlap was known.

The interface that was created for this thesis is shown in Fig. 16. In this application first step is to choose a folder with the tiled images. All images must be the same size and type (png, tiff and jpg are supported). For the mosaic building the amount of rows and columns – as well as the stitching pattern and the starting point of the stitching – must be known. If the images overlap, the overlap number needs to be placed either in pixels of percentages.

In addition to these it is possible to do flat-field correction, contrast enhancement (increases the contrast) or Fourier filtering to the image. The flat-field correction – where the intensity around the image is set to equal value – can be useful especially in the case that the tiles have strong vignetting for example due to the camera lens. The flat-field correction is done to each tile individually. The Fourier filtering has a similar effect and it is also meant to even out the intensity across the image. Fourier filtering in this case is done for the stitched mosaic. As an example of a built mosaic that has been flat-field corrected, the Fig. 15 is presented. The colored areas were added after the processing for the presentation of the scanned areas.

This application was used in the study for the comparison of heavy ions and pulsed laser. From the pulsed laser scan for the LM124, the tile images were acquired.

These tiles were built as a mosaic with the Matlab application and the resulting image can be seen in the Fig. 17. This mosaic was used to identify and show the places of the transistors that were studied for the SET comparison. With the circuit diagram of the LM124 shown in Fig. 4 and by comparing this to several previous studies [17, 20], it was possible to name the transistors in the built mosaic. This made the pulsed laser analysis with SEESIM much easier.

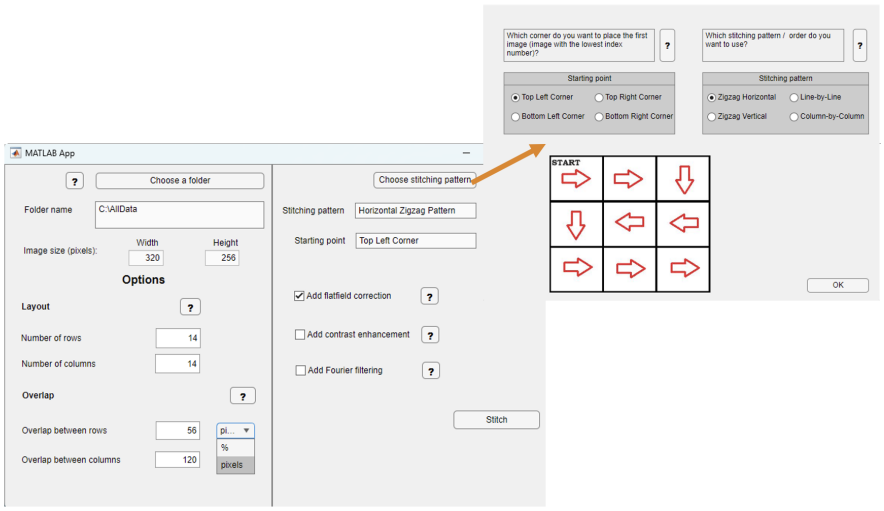

Figure 16. Matlab interface created for the mosaic building of tiled images.

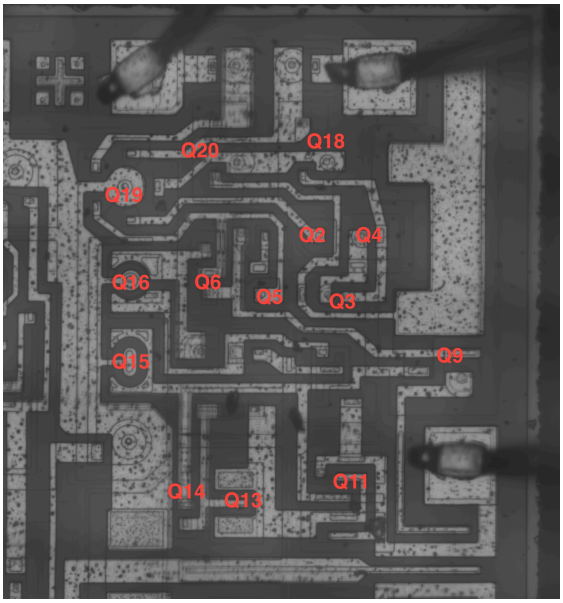

Figure 17. Mosaic image built with the Matlab interface with the transistors named in the image.

4 Results

In this section the results for both heavy ion and pulsed laser testing are processed and analyzed. As the results and obtained effects were different for the two studied devices (LM124 and 23LCV512), the data was also analyzed in different ways. When possible, the analyzed data was compared between the heavy ion and pulsed laser testing.

4.1 Analysis of the LM124 data

Five different LET values (shown in Table 1) were used in order to obtain transients from the LM124 with heavy ions. With the lower LETs it can be seen that the amount of transients was clearly lower. The SET cross sections are presented as a function of LET in Fig. 18. These cross sections were calculated with the equation 1. For the amount of events, the used value was the total number of transients collected for each LET with the fluence of 10^6 ions/cm^2.

In Fig. 18 the error estimations for SET cross sections are also presented. The errors were calculated with the equation 2 where the error for number of events was considered to follow Poisson's distribution. Thus the error for events was estimated by using the equation 3. Error for the fluence was approximated to be ± 10 %. In this graph it can be seen that the error is much higher for the lower LETs which seems like a reasonable result since for these LETs much less data was collected and thus the error margin increased.

In Fig. 18, the cross sections calculated with the amount of acquired transients is shown. For lower LETs, such as carbon, lower cross section is observed. At higher LETs, like xenon and krypton, saturation begins to occur, and the cross sections no longer exhibit significant changes with increasing LET. It is important to note that there is some possible error in these results. For instance, since no transients are observed with neon, which has a higher LET than carbon, the error margin might be the reason why a lower LET gives us transients while the higher one does not.

Fig. 18 shows that the obtained SET cross section does have similar shape and

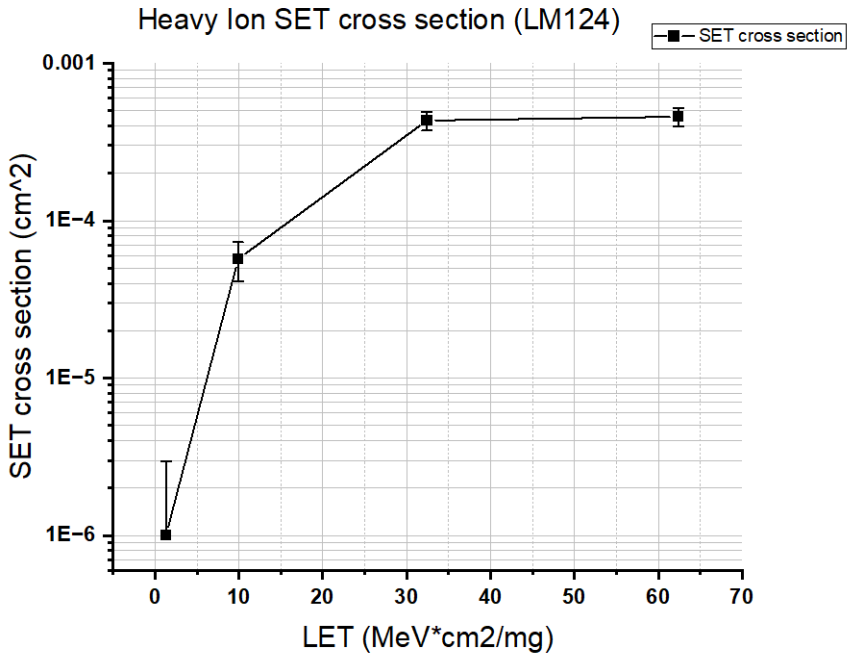

Figure 18. SET cross sections calculated from the heavy ion data presented as a function of LET (flux of $1.5{\cdot}10^4$ ions/(s cm^2) and fluence of 10^6 ions/cm^2).

values compared to the previously measured SET cross section versus LET graph found from the literature [21]. This previous study was done to the same operational amplifier as used here. When comparing these graphs it is possible to see that the saturation starts around the LET of 30 MeV/(mg/cm^2) and the cross section stays around the same after this. The cross section value reached in both this study and the compared article is around 10^{-3} cm^2. Overall, when comparing the results in this study to the literature, the results for the heavy ion testing looked promising.

From the heavy ion data several different shaped pulses were observed. However, with just this data it is not possible to connect the pulse shapes to specific transistors. This is where the pulsed laser testing analysis is needed. After the laser testing – which has been detailed in Section 3.4.1 – the analysis was done for the laser data with SEESIM. In SEESIM the heat map (Fig. 13) gave the locations of the most sensitive areas in the amplifier. By pressing a certain spot in the heat map a type of SET pulse specific to that area was shown. Just like with heavy ion testing several different shapes of pulses were shown across the device. The parameters used for the laser testing can be found in Table 2.

The mosaic image representing the layout of LM124 with the transistor places

located (Fig. 17) was used as a map for finding the specific transistors. When the transistor locations were known it was possible to press this location in SEESIM and connect a pulse shape to a transistor. From the heavy ion data it was possible to divide the pulse shapes in four categories. When studying the response from the pulsed laser data the different transistors could also be categorized into these four groups. The distribution of transistors in different groups is described in Table 3.

Group	Transistor(s)
A	Q18
B	Q9, Q11, Q19
C	Q2, Q3, Q4, Q5, Q20
D	Q13, Q14

Table 3. The classification of the transistors according to their pulse shape.

The four groups of laser pulse shapes are shown in Fig. 19 with the xenon pulses showed in red and the laser pulses in black and blue. Here only the transistors that gave clear pulses were compared. The heavy ion data was obtained by using xenon ions.

In Fig. 19 the group A type pulses were only found from the area of Q18. In the heavy ion data this pyramid shape was only seen with very low amplitudes. Around Q18 these low amplitude shapes were most common but higher amplitudes could also be acquired with the pyramid shape. In this pulse shape it could be seen that with the same amplitude, the laser data gave always pulses with larger width compared to the heavy ion data.

For the group B it can be seen that the transistors Q11 and Q19 give a pulse shape very close to the one obtained from the heavy ion data. Transistor Q9 gave also a negative pulse but as can be seen the width of the pulse was clearly larger. Also for the Q13 and Q14, in the group D, very similar pulse shapes are found between the heavy ion and laser testing. However, in this case we did have more changes in the amplitude in both heavy ion and pulsed laser data even though the shape stayed the same.

Much like with the group A, the group C also shows larger width for the laser data when the same amplitude is considered. Group C, which contains Q2, Q3, Q4, Q5 and Q20, has more variations in the pulsed laser data shapes than the other groups. Even though the laser data did vary, the pulses were placed under the same category as the heavy ion data was not possible to be divided into more groups. All

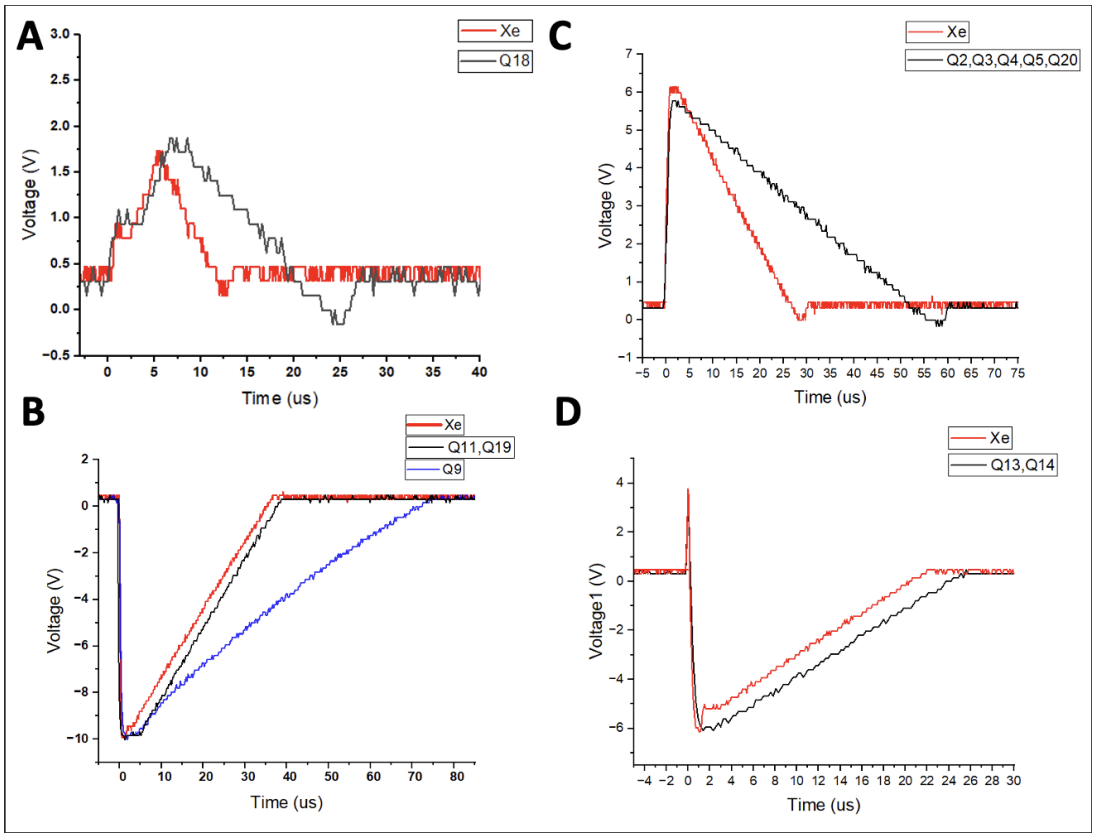

Figure 19. Comparison of Xe and pulsed laser induced SETs divided into four groups based on the shape of the transient.

the pulses in both heavy ion and laser data had a positive amplitude and a small dip to the negative values. The laser data could also be categorized under the same group because those pulses had constantly wider widths compared to the heavy ion data with the same amplitudes.

In addition to comparing the heavy ion and laser data with each other, the data could also be compared to a similar study done before. In [20] the same device (LM124) was irradiated with heavy ions and pulse-laser and as a result it can be seen that similar pulse shapes were acquired. Few different transistors were covered here that were not part of the previous study and vice versa. For the group A and B graphs it is possible to see similar shapes – with the exception that Q11 was not studied before. In both studies also the shape of the group D was found. However, in [20] this shape was identified from the transistor Q16 from which in this study we did not get clear pulse shape.

Another difference between these studies was that in [20] Q20 was separate from

the rest of the group C. For this study the heavy ion data did not present clear enough differences for the positive pulses in this category. Even though with the pulsed laser data alone the separation could have done, it was not possible when heavy ion data was considered as well. The possible reason for the differences between these shapes could be the changes in the manufacturing. Since the article was made in 2004, it is possible that some changes have happened since this. One reason to suspect this is the observed changes in the layout of the device. This can be seen when comparing Fig. 17 in this study and the equivalent photomicrograph of LM124 presented in the article [20]. Between these layouts it can be seen that the physical appearance of the device has changed so it is possible that the functionality of the transistors has changed as well.

Now that the heavy ion data has been connected to specific transistors, it can be also useful to compare the amount of pulses obtained for different shapes and different ions. In Fig. 20 the amount of pulse shapes is shown as a histogram. These transients were observed with the flux of $1.5 \cdot 10^4$ ions/(s cm^2) and the fluence of 10^6 ions/cm^2.

From Fig. 20 it can be seen that the shapes of group C and D are the most seen pulses in the heavy ion data. Partly this can be because the trigger level in PicoScope was set to +2 V. This meant that the first transients recorded had to always have the minimum amplitude of +2 V. Therefore, in addition it was possible to obtain transients with lower or negative amplitudes only after the first transient was triggered. This means that the group A and B pulses were never seen as the first transient in the PicoScope data but rather as an additional transients. The high amount of group C could also be explained with the fact that this group covers several transistors.

In the histogram the differences between the ions can also be studied. Between xenon and krypton we have very similar amount of pulses in all the categories. This also aligns well with the SET cross section results where the saturation happened around these values of LET. For argon only the group C and D SETs were seen. An interesting feature about the argon data was that the group C pulses were clearly observed more than group D pulses whereas for krypton and xenon data group D was the largest and the difference was not so clear. In the histogram the one carbon pulse is shown and it is in the shape group C.

For the pulse shape groups C and D, the SET cross section graphs are shown

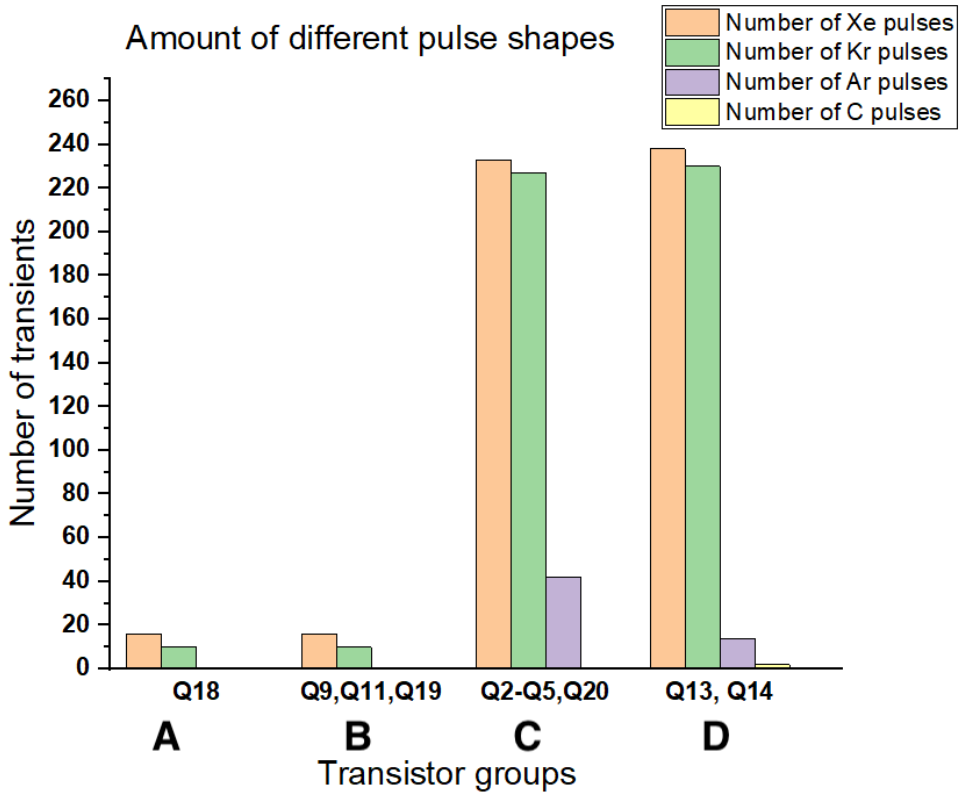

Figure 20. Histogram presentation for the distribution of different pulse types collected with the flux of $1.5*10^4$ ions/(s cm^2) and fluence of 10^6 ions/cm^2.

together with the total SET cross section graph in Fig. 21. In this figure it can be seen that for the group D the SET cross section has the same shape as for the total cross section. For the group C the argon value is slightly higher as could be seen from Fig. 20 as well. This could mean that in the group C there are transistors that are more sensitive since the lower LET is enough to trigger this type of SETs.

The SET cross sections in Fig. 21 were calculated with the equation 1. The error estimation was done similarly to the Fig. 18 with the equation 3 for the error of the number of events and 2 for the whole cross section. Here it can be seen that the error bars are much higher for the argon cross sections. This is due to the fact that for argon, much less events were detected even though the fluence remained the same.

Because of the technical constraints, only one trigger level was used meaning that for the groups A and B it is impossible to know the actual number of events since these were never triggered as the main transient. This is why the cross sections were not calculated for the groups A and B since the value calculated with this number of events would not be accurate.

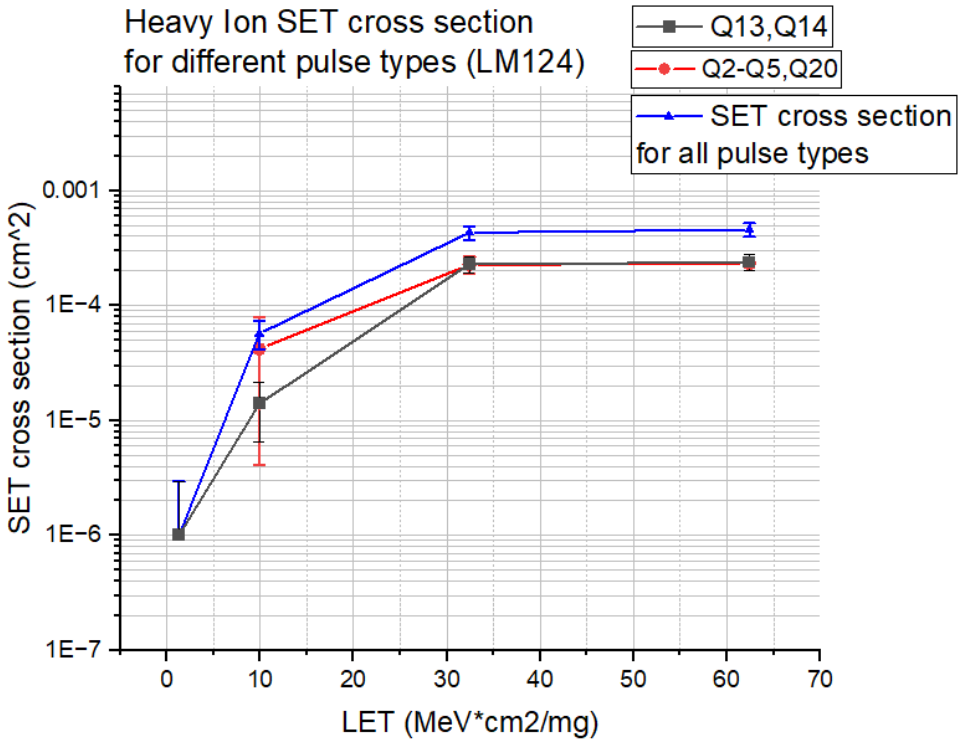

Figure 21. SET cross sections for the most commonly seen pulse types and the total SET cross section presented as a function of LET (flux of $1.5 \cdot 10^4$ ions/(s cm^2) and fluence of 10^6 ions/cm^2).

There could be many possible reasons for why we see certain type of pulses with the heavy ion. Some transistors could be more sensitive to the radiation and especially in the groups with multiple transistors it is possible that some contribute more than others. Also the shapes seen with the lower LETs are interesting for the analysis, as it can be so that these transistors that show pulses even with the lower LET are more sensitive.

4.2 Analysis of the 23LCV512 data

The second device – 23LCV512 – in this study was a memory hence the data collected from this was SEU data. SEUs were detected with several different LETs during the heavy ion testing. This part of the study was built on top of previously collected data from a study done by Radtest Ltd for the same device. By using this data as a reference, low enough values for flux (10^3 ions/(s cm^2)) and fluence (10^5 ions/cm^2) were chosen to avoid SELs and to ensure the detection of SEUs. For the higher LET

these values were lowered even more to avoid latchups. The SEUs detected with the heavy ion testing were mostly SBUs but few MBUs (2-bit or 3-bit upsets) were also detected. SEUs were detected with carbon, neon and argon, which were also used in the previous data along with aluminium. LET values for these can be found from Table 1.

With the amount of SEUs and the reached fluence, the SEU cross sections can be calculated. For the calculation of the SEU cross section the equation 1 was used as follows

$$\sigma_{SEU} = \frac{N_{SEU}}{\Phi}. \tag{9}$$

where the amount of SEUs and the reached fluences from different runs were summed for each LET value. The SEU cross sections for the heavy ion data are presented as a function of LET in Fig. 22.

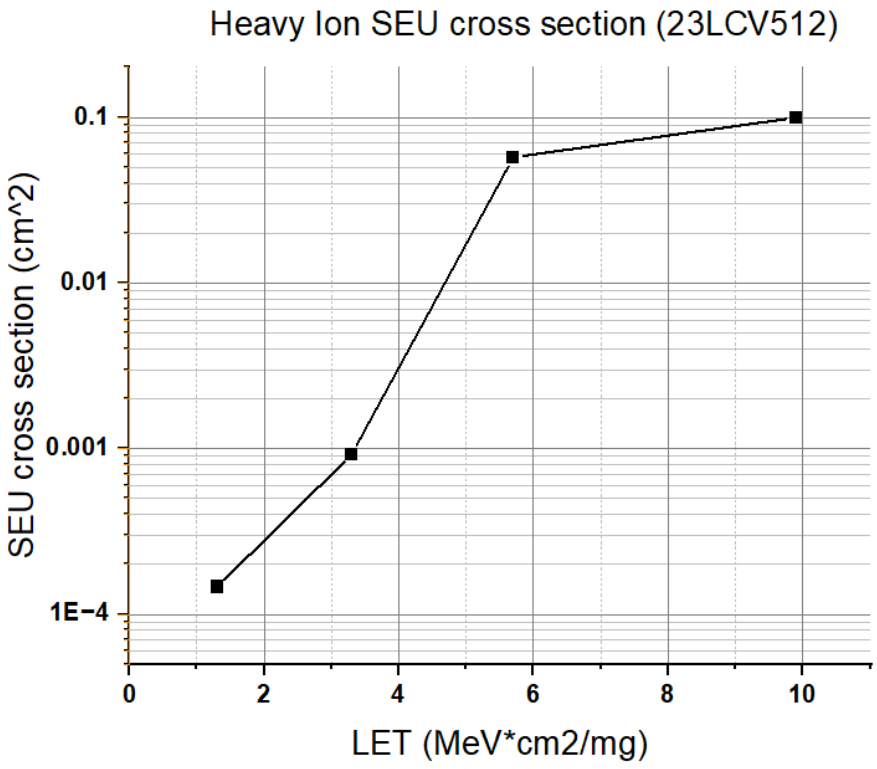

Figure 22. SEU heavy ion cross section as a function of LET (flux of 10^3 ions/(s cm^2) and fluence of 10^5 ions/cm^2).

As can be seen from Fig. 22, the cross section increases rapidly after neon (LET

= 3.3 MeV/(mg/cm^2)) and at the LETs around 10 MeV/(mg/cm^2) the growth slows down. So around the LET of 10 MeV/(mg/cm^2) it is possible that some saturation is already seen. However, it is important to note that there is an amount of uncertainty in this measurement. Good implication for this data was that it aligned well with the data from the company's previous study. The new study added the argon data to the previous values which shows the possible saturation at approximately LET of 10 MeV/(mg/cm^2). This could not be seen previously as the highest LET was for aluminium (LET = 5.7 MeV/(mg/cm^2)). The previously acquired results also supported this study since aluminium was a good addition to show the possible behavior of the cross section between neon and argon.

Since no similar previous study for the 23LCV512 has been published, there is no literature data to compare this directly to. For other types of SRAM memories, this type of SEU analysis has been done and in [22] is shown similar graphs for other SRAM memories. Even though the devices are different, it is possible to see similarities between these SEU cross sections. In both this study and [22] the cross sections increase rapidly up to the LET of 10 MeV/(mg/cm^2). In both studies the cross section values around this LET are in between 0.01 cm^2 and 0.1 cm^2.

The previously conducted SRAM study for the 23LCV512 at Radtest Ltd was done only with heavy ions as mentioned earlier. Now in addition to this, pulsed laser SEU data was acquired in this study. When scanning the sensitive area of the device with different pulse energies, a threshold for triggering SEUs could be found from between 1.01 nJ and 2.13 nJ. With 1.01 nJ, no SEUs were detected while scanning the sensitive area. The entire chip was also scanned with the 1.01 nJ energy to make sure of the threshold and no SEUs were detected this time either. For the 2.13 nJ, 4.08 nJ and 6.23 nJ scans we were able to trigger SEUs. However, since the test method was originally designed for heavy ion testing the results were not exactly in the same format as for the heavy ions.

From the laser data, it was observed that, instead of acquiring mostly SBUs – as happened in the heavy ion testing – the majority of the data consisted of 4-bit upsets. With closer examination, it was found that this occurs because once a reading exhibits a 4-bit upset, all subsequent addresses remain at the altered value. In this case, the checkerboard pattern (01010101) written to the memory changes to all ones (11111111). One possible reason for this could be that, unlike with heavy ions, the upsets are not being triggered in the memory cells. Currently, upsets are

being observed only on the side of the chip, as shown in blue in Fig. 15. However, the areas where SEUs are triggered by heavy ions are probably in the memory cell areas, marked as red in Fig. 15. These areas have metallization, meaning that with front-side testing, which was conducted here, it is not possible to cause any effects in those areas when using the laser.

Because the SRAM gives all ones after an effect happens, total of millions of upsets are obtained from the Python calculator. Since most of these upsets happen after one change in the address, the amount of upsets acquired with the heavy ions and with the laser are not comparable in the same way. Instead of looking at the amount of SEUs that can calculated from the laser data, it is possible to look at the amount of readings that have upsets. This is a better way to examine the laser results since the change from the checkerboard to all ones only happens once per reading.

There is a level of uncertainty that comes to the measurement from looking at only the amount of readings. After the 4-bit flip happens the value can not change anymore until new reading is done. This means that if another SEU would happen after the reading has already changed value once, the second SEU would not be recorded. This increases the dead time of the measurement. Besides this there is also dead time during the read and write operations in which the SEU would not be recorded. With the read operation the dead time means that the SEU can happen in the area that has already been read and saved in a READ file. With the write operation if the SEU happens before writing, the write operation can rewrite on top of the SEU data. In both of these cases the dead time can be approximated to be about half of the operation time.

With the laser, there is no clear fluence like with heavy ions. However, with the equation 8 the equivalent fluence could be calculated. In this equation the frequency, summed scan times and the scan area were known. Since it was possible to obtain the equivalent fluence, the SEU cross section for pulsed laser testing could also be calculated. For this the equation 7 was used as follows

$$\sigma_{SEU} = N_{SEU} \cdot \frac{S}{f t_{scan}}. \tag{10}$$

In this equation the N_{SEU} was the summed amount of all the SEUs (or in this case amount of all the readings that had SEUs) for each energy, S was the scan area (shown blue in Fig. 15), f was the pulse frequency and t_{scan} was the summed scan

time of all the measurements. When considering the scan time, the dead time needed to be taken into account. Because of the read and write operations, the dead time was approximated to be half of the scan time and this was reduced from the total scan time.

The cross sections were calculated with the amount of readings that showed SEUs. These cross sections are shown in Fig. 23 as a function of LET. From this figure it can be seen that the cross sections are much lower for the laser than for the heavy ions which can be partly because only the side of the chip can be effected with the laser. Some similarities can be seen with the graph shapes between laser and heavy ion data as the lower pulse energies offer a possibility for higher increase of the cross section while with the higher pulse energies the development starts to flatten slightly.

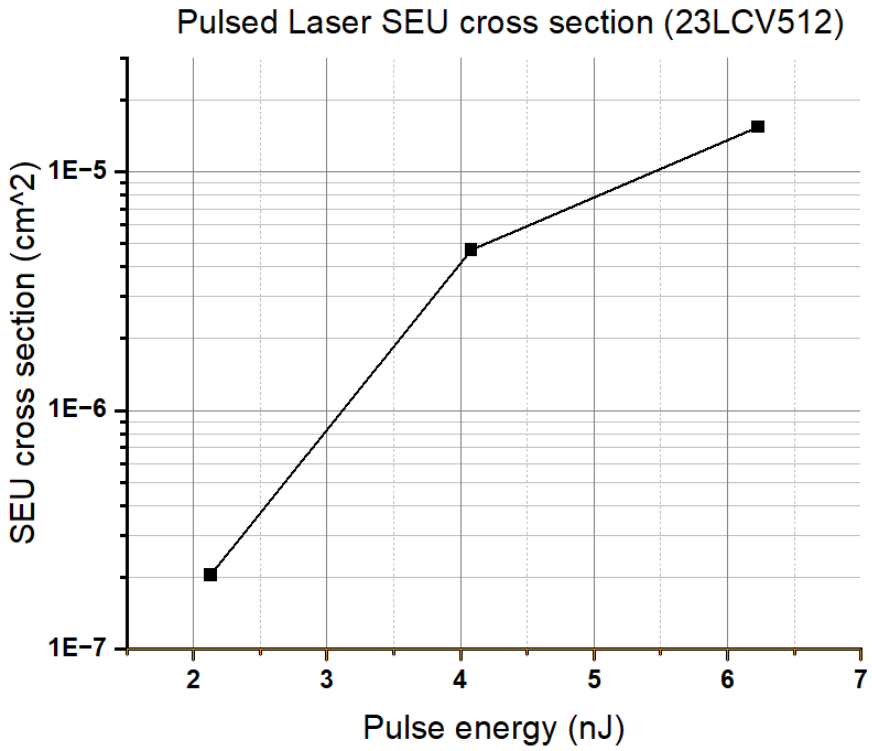

Figure 23. SEU laser cross section as a function of the laser pulse energy.

For the laser testing of 23LCV512 there could be few useful developments for the future. In order to understand the SEU trend better it might be good to add even higher energies to see if the curve does in fact saturate. However, since with 6.23 nJ we did already acquire millions of SEUs it could be a problem to go to even

higher energies without destroying the device. Another possible improvement for this SEU testing could be to do backside testing for the device. Since the metallization of the cell memory areas could be a reason why we do not get similar SEU data compared to the heavy ion testing, performing a backside testing could help. Also for SEL study the backside testing might be a great possibility. The development of the methodology and possibly reducing the dead time could also help with the SEU study. One option for reducing the dead time could be by slowing the scanning pace in order to tune the C++ code better to the rhythm of the laser. The problem in this is that it can be very time consuming.

5 Conclusions

The results obtained from this study gave some good comparison data for the heavy ions and pulsed laser testing. Especially since for this specific laser system, SEREEL2, this type of comparison study has not been done before so this study gives a good base for future work. For Radtest Ltd this study also provided the mosaic building code in addition to the obtained data.

For the LM124, the heavy ion testing revealed that SET cross sections increase with the LET values up to a certain point, after which saturation occurs. This is consistent with literature findings where saturation typically begins around a LET of 30 MeV/(mg/cm^2) [21]. The study also showed that the different pulse shapes were possible to be compared from the pulsed laser and heavy ion data. The shapes connected reasonably well between the two testing methods and similarities could be seen with a previous study [20] done for the same device.

The analysis of 23LCV512 SRAM highlighted the challenges in correlating SEU cross sections from heavy ion and laser testing. Unlike with LM124 testing, with 23LCV512 it was noted that the same testing setup did not work perfectly for both methods. With the heavy ion data, it is possible to create SEU cross section graph that is similar to SEU cross sections observed in literature [22]. Since the laser and heavy ion data were not in the same format, the comparison between these methods was not entirely comprehensive. In order to obtain better results from the laser testing the SEU collecting code could be tuned to match the laser setup better.

Overall, the study suggests that some promising comparison results can be obtained from between the SEREEL2 pulsed laser testing system and heavy ion data. With some tuning on the test methods – especially for 23LCV512 – even more accurate data could be observed.

6 Future Work

As already mentioned in Section 5 there are several possible options to further continue this study. For the LM124, an interesting continuation could be to study the dependence of laser pulse energies and LET with the SEREEL2. Seeing how the different pulse shapes act as the laser pulse energy is changed, could give some interesting results. One question in this would be whether similar effect as with the heavy ions – where high LET gives larger variety different shapes than low LET – is observed with laser testing. This way it might be possible to see further which transistors are most sensitive and if this kind of analysis is possible to do with pulsed laser.

For 23LCV512 study, there are several possible ways to further develop the testing. In the testing method itself the practical way of developing it further would be to integrate the SEU collecting code and the SEU calculator. This could help with both the heavy ion and laser testing. Also the code could be tuned better for the laser testing purposes. Adjusting the laser testing parameters – by for example increasing the pulse duration – could reduce dead time and give better results. Though it is good to note that this will also increase the overall scan time so its usefulness is dependent on the purposes of the future study. Overall, compared to the LM124 study, the method of the 23LCV512 study itself could use more development in the future.

One useful approach for the future study of the 23LCV512 – or similar memory devices – could be backside testing. In order to get comparable data from both heavy ion and pulsed laser testing the same parts need to be hit. Since currently the metallization of the front-side is the problem when it comes to hitting the memory cell areas, doing the testing from the backside could be a solution for this. Thus backside testing could provide more comparable data.

References

[1] L. Edmonds, C. Barnes, and L. Scheick. *An Introduction to Space Radiation Effects on Microelectronics*. Jet Propulsion Laboratory, National Aeronautics and Space Administration, 2000.

[2] A. Bijola. "Interaction of Radiation with Matter". *Practical Radiation Oncology*. Ed. by S. Mallick, G. K. Rath, and R. Benson. Springer, Singapore, 2020. DOI: 10.1007/978-981-15-0073-2_1.

[3] A. Javanainen. "Particle radiation in microelectronics". PhD thesis. University of Jyväskylä, 2012.

[4] S. P. Buchner et al. "Pulsed-Laser Testing for Single-Event Effects Investigations". *IEEE Transactions on Nuclear Science* 60.3 (2013), pp. 1852–1875. DOI: 10.1109/TNS.2013.2255312.

[5] R. D. Schrimpf et al. "Physical mechanisms of single-event effects in advanced microelectronics". *Nuclear Instruments and Methods in Physics Research Section B: Beam Interactions with Materials and Atoms* 261.1–2 (2007), pp. 1133–1136. DOI: 10.1016/j.nimb.2007.04.050.

[6] R. Gaillaird. "Single Event Effects: Mechanisms and Classification". *Soft Errors in Modern Electronic Systems*. Ed. by M. Nicolaidis. Springer, Boston, MA, 2011. DOI: 10.1007/978-1-4419-6993-4_2.

[7] F. W. Sexton. "Destructive single-event effects in semiconductor devices and ICs". *IEEE Transactions on Nuclear Science* 50.3 (2003), pp. 603–621. DOI: 10.1109/TNS.2003.813137.

[8] K. Tapero. "Single-Event Effects Test Methods". *Radiation Effects on Integrated Circuits and Systems for Space Applications*. Ed. by R. Velazco, D. McMorrow, and J. Estela. Springer, Cham, 2019. DOI: 10.1007/978-3-030-04660-6_3.

[9] J. R. Taylor. *Introduction To Error Analysis: The Study of Uncertainties in Physical Measurements, second edition*. University Science Books, 1997.

[10] W. E. Ricker. “The Concept of Confidence or Fiducial Limits Applied to the Poisson Frequency Distribution”. *Journal of the American Statistical Association*. Ed. by R. Velazco, D. McMorrow, and J. Estela. Taylor Francis, Ltd., 2019. DOI: 10.1007/978-3-030-04660-6_3.

[11] A. Ostendorf and K. König. “Tutorial: Laser in material nanoprocessing”. *Optically Induced Nanostructures: Biomedical and Technical Applications* (2015).

[12] S. P. Buchner et al. “Laser Simulation of Single Event Upsets”. *IEEE Transactions on Nuclear Science* 34.6 (1987), pp. 1227–1233. DOI: 10.1109/TNS.1987.4337457.

[13] P. Fouillat et al. “Fundamentals of the Pulsed Laser Technique for Single-Event Upset Testing”. *Radiation Effects on Embedded Systems*. Ed. by R. Valezco, P. Fouillat, and R. Reis. Springer, Dordrecht, 2007. DOI: 10.1007/978-1-4020-5646-8_6.

[14] A. H. Johnston. “Charge Generation and Collection in p-n Junctions Excited with Pulsed Infrared Lasers”. *IEEE Transactions on Nuclear Science* 40.6 (1993), pp. 1694–1702. DOI: 10.1109/23.273491.

[15] C. A. Gossett, B. W. Hughlock, and A. H. Johnston. “Laser Simulation of Single-Particle Effects”. *IEEE Transactions on Nuclear Science* 39.6 (1992), pp. 1647–1653. DOI: 10.1109/23.211348.

[16] F. R. Palomo et al. “Pulsed Laser SEU Cross Section Measurement Using Coincidence Detectors”. *IEEE Transactions on Nuclear Science* 56.4 (2009), pp. 2001–2007. DOI: 10.1109/TNS.2009.2018274.

[17] S. P. Buchner et al. “The Effects of Low Dose-Rate Ionizing Radiation on the Shapes of Transients in the LM124 Operational Amplifier”. *IEEE Transactions on Nuclear Science* 55.6 (2008), pp. 3314–3320. DOI: 10.1109/TNS.2008.2007952.

[18] *23LCV512 - 512-Kbit SPI Serial SRAM with Battery Backup and SDI Interface*. DS20005157. Microchip. 2012–2023.

[19] G. Berger et al. “CYCLONE – A Multipurpose Heavy Ion, Proton and Neutron SEE Test Site”. *Abstracts for RADECS 97 W-25*. 1997.

[20] S. Buchner et al. “Comparison of single-event transients induced in an operational amplifier (LM124) by pulsed laser light and a broad beam of heavy ions”. *IEEE Transactions on Nuclear Science* 51.6 (2004), pp. 2776–2781. DOI: 10.1109/TNS.2004.835111.

[21] S. P. Buchner et al. “Pulsed-Laser Testing Methodology for Single Event Transients in Linear Devices”. *IEEE Transactions on Nuclear Science* 51.6 (2004), pp. 3716–3722. DOI: 10.1109/TNS.2004.839263.

[22] L. Scheick, G. Swift, and S. Guertin. “SEU Evaluation of SRAM Memories for Space Applications”. *IEEE Radiation Effects Data Workshop. Workshop Record. Held in conjunction with IEEE Nuclear and Space Radiation Effects Conference*. 2000, pp. 61–63. DOI: 10.1109/REDW.2000.896270.